for use as mass, force, and charge sensors (*22*–*28*). The application of graphene NEMS extends beyond just mechanical resonators. This robust conducting membrane can act as a nanoscale supporting structure or atomically thin membrane separating two disparate environments.

References and Notes

1. H. G. Craighead, *Science* **290**, 1532 (2000).
2. K. L. Ekinci, M. L. Roukes, *Rev. Sci. Instrum.* **76**, 061101 (2005).
3. B. T. Kelly, *Physics of Graphite* (Applied Science, London; Englewood, NJ, 1981).
4. M. Wilson, *Phys. Today* **59**, 21 (2006).
5. K. S. Novoselov *et al.*, *Proc. Natl. Acad. Sci. U.S.A.* 10451 (2005).
6. K. S. Novoselov *et al.*, *Nature* **438**, 197 (2005).
7. Y. B. Zhang, Y. W. Tan, H. L. Stormer, P. Kim, *Nature* **438**, 201 (2005).
8. J. S. Bunch, Y. Yaish, M. Brink, K. Bolotin, P. L. McEuen, *Nano Lett.* **5**, 287 (2005).
9. Materials and methods are available as supporting material on *Science* Online.
10. A. C. Ferrari *et al.*, *Phys. Rev. Lett.* **97**, 187401 (2006).
11. A. Gupta, G. Chen, P. Joshi, S. Tadigadapa, P. C. Eklund, *Nano Lett.* **6**, 2667 (2006).
12. D. Graf *et al.*, http://arxiv.org/PS_cache/cond-mat/pdf/0607/0607562.pdf (2006).
13. V. Sazonova *et al.*, *Nature* **431**, 284 (2004).
14. S. Timoshenko, D. H. Young, W. Weaver, *Vibration Problems in Engineering*. (Wiley, New York, ed. 4, 1974), pp. 425–427.
15. D. Qian, G. J. Wagner, W. K. Liu, M. F. Yu, R. S. Ruoff, *Appl. Mech. Rev.* **55**, 495 (2002).
16. L. Sekaric *et al.*, *Appl. Phys. Lett.* **81**, 4455 (2002).
17. X. X. Li, T. Ono, Y. L. Wang, M. Esashi, *Appl. Phys. Lett.* **83**, 3081 (2003).
18. K. Y. Yasumura *et al.*, *J. Microelectromech. Syst.* **9**, 117 (2000).
19. S. S. Verbridge, J. M. Parpia, R. B. Reichenbach, L. M. Bellan, H. G. Craighead, *J. Appl. Phys.* **99**, 124304 (2006).
20. R. J. Schoelkopf, P. Wahlgren, A. A. Kozhevnikov, P. Delsing, D. E. Prober, *Science* **280**, 1238 (1998).
21. M. D. LaHaye, O. Buu, B. Camarota, K. C. Schwab, *Science* **304**, 74 (2004).
22. B. Ilic *et al.*, *J. Appl. Phys.* **95**, 3694 (2004).
23. N. V. Lavrik, P. G. Datskos, *Appl. Phys. Lett.* **82**, 2697 (2003).
24. K. L. Ekinci, X. M. H. Huang, M. L. Roukes, *Appl. Phys. Lett.* **84**, 4469 (2004).
25. T. Kenny, *IEEE Sensors J.* **1**, 148 (2001).
26. A. N. Cleland, M. L. Roukes, *Nature* **392**, 160 (1998).
27. R. G. Knobel, A. N. Cleland, *Nature* **424**, 291 (2003).
28. T. P. Burg, S. R. Manalis, *Appl. Phys. Lett.* **83**, 2698 (2003).

29. We thank C. Umbach and L. Bellan for help with Raman spectroscopy; R. Reichenbach for help with the laser setup and the schematic in the Supporting Online Material; and P. Kim, Y. Zhang, R. Ilic, and K. Schwab for useful discussions. This work was supported by the NSF through the Center for Nanoscale Systems and the Cornell Center for Materials Research, and by the Microelectronics Advanced Research Corporation Focused Research Center on Materials, Structures, and Devices. Sample fabrication was performed at the Cornell Nanoscale Science and Technology Facility, a National Nanotechnology Infrastructure Network node, funded by NSF.

Supporting Online Material

www.sciencemag.org/cgi/content/full/315/5811/490/DC1
Materials and Methods
SOM Text
Figs. S1 to S3
References

27 October 2006; accepted 11 December 2006
10.1126/science.1136836

Improved Oxygen Reduction Activity on $Pt_3Ni(111)$ via Increased Surface Site Availability

Vojislav R. Stamenkovic,[1,2]* Ben Fowler,[3] Bongjin Simon Mun,[2] Guofeng Wang,[4] Philip N. Ross,[2] Christopher A. Lucas,[3] Nenad M. Marković[1]*

The slow rate of the oxygen reduction reaction (ORR) in the polymer electrolyte membrane fuel cell (PEMFC) is the main limitation for automotive applications. We demonstrated that the $Pt_3Ni(111)$ surface is 10-fold more active for the ORR than the corresponding Pt(111) surface and 90-fold more active than the current state-of-the-art Pt/C catalysts for PEMFC. The $Pt_3Ni(111)$ surface has an unusual electronic structure (*d*-band center position) and arrangement of surface atoms in the near-surface region. Under operating conditions relevant to fuel cells, its near-surface layer exhibits a highly structured compositional oscillation in the outermost and third layers, which are Pt-rich, and in the second atomic layer, which is Ni-rich. The weak interaction between the Pt surface atoms and nonreactive oxygenated species increases the number of active sites for O_2 adsorption.

When a polymer electrolyte membrane fuel cell (PEMFC) is used in a demanding application such as an automobile, it must overcome the kinetic limitations on the oxygen reduction reaction (ORR), which have led to three fundamental problems (*1*–*5*). First, the substantial overpotential for the ORR (*6*–*10*) at practical operating current densities reduces the thermal efficiency well below the thermodynamic limits, typically to about 43% at 0.7 V [versus the theoretical thermal efficiency of 83% at the reversible potential for the ORR (1.23 V)]. Second, an approximately fivefold reduction of the amount of Pt (platinum-loading) in current PEMFC stacks is needed to meet the cost requirements for large-scale automotive applications (*10*). Finally, the dissolution and/or loss of Pt surface area in the cathode must be greatly reduced.

These limitations could be eliminated if stable cathode catalysts, with an order of magnitude increase in the specific activity over that of state-of-the-art Pt/C catalysts, can be developed (*10*). In the hope that a combination of different metals would have improved catalytic activity and stability relative to those of a pure metal, the ORR has been studied on numerous bi- or multimetallic alloys (*6*, *8*, *11*–*17*). These studies have led to incremental improvements to catalyst performance, but large increases in activity have yet to be realized.

Rather than use a trial-and-error or combinatorial approach, we have examined selected cathode materials with well-characterized surfaces so that the mechanism of action can be attributed to a specific property (at the atomic and molecular level) of the surface under study. In this way, we can determine (i) whether the kinetics of the ORR are structure-sensitive, (ii) the composition of the topmost surface atomic layers (the segregation profile), and (iii) how alloying [usually described in terms of the ligand effect or/and ensemble effect (*18*–*20*)] alters the chemical properties of the surfaces. Similar approaches are commonly used in gas-phase catalysis (*21*) under ultrahigh vacuum (UHV) and near-ambient conditions, but alloy surface chemistry on single-crystal surfaces at electrochemical interfaces is relatively unexplored. These aqueous interfaces are more complex in that they necessarily contain solvent and electronic/ionic charge, and (experimentally) it is very challenging but still tractable to use in situ surface-sensitive methods to characterize potential-induced changes in the surface properties and reactivity.

We have used a combination of ex situ and in situ surface-sensitive probes and density functional theory (DFT) calculations to study the ORR on $Pt_3Ni(hkl)$ single-crystal surfaces, identify which surface properties govern the variations in reactivity of PtNi catalysts, and determine how surface structures, surface segregation, and intermetallic bonding affect the ORR kinetics. Well-characterized PtNi single-crystal electrode surfaces were formed and characterized with UHV methods for surface preparation and surface analysis. These surfaces were transferred into the electrochemical environment without airborne contamination, and the stability of the UHV-prepared

[1]Materials Science Division, Argonne National Laboratory, Argonne, IL 60439, USA. [2]Materials Sciences Division, Lawrence Berkeley National Laboratory, University of California, Berkeley, CA 94720, USA. [3]Oliver Lodge Laboratory, Department of Physics, University of Liverpool, Liverpool, L69 7ZE, UK. [4]Department of Chemistry and Physics, University of South Carolina, Aiken, SC 29801, USA.

*To whom correspondence should be addressed. E-mail: vrstamenkovic@anl.gov (V.R.S.); nmmarkovic@anl.gov (N.M.M.)

surface was determined with a combination of in situ surface-sensitive probes with electrochemical methods so that activity relationships could be obtained in real time.

The results of the preparation and characterization of $Pt_3Ni(hkl)$ alloy surfaces in UHV are summarized in Fig. 1. The surface-sensitive techniques that were used included low-energy electron diffraction (LEED), Auger electron spectroscopy (AES), low-energy ion scattering (LEIS), and synchrotron-based high-resolution ultraviolet photoemission spectroscopy (UPS) (see methods in the supporting online material). Each of these methods has certain advantages, and they yield complementary information. The surface symmetry obtained from LEED analysis shows that, whereas the $Pt_3Ni(111)$ surface exhibits a (1 × 1) pattern (Fig. 1D) (i.e., that of the bulk termination), the atomically less dense $Pt_3Ni(100)$ surface shows a (1 × 5) reconstruction pattern (the so-called "hex" phase) in both the [011] and [01-1] directions (Fig. 1E). Analysis of the $Pt_3Ni(110)$ LEED data (Fig. 1F) indicates that this surface may exhibit a mixture of (1 × 1) and (1 × 2) periodicities, the latter being known as the (1 × 2) missing-row structure (*22*).

The composition of the outermost atomic layer was obtained with LEIS, as previously shown for Pt_3Ni polycrystalline alloys (*15*, *23*); after a final anneal, the surface atomic layer of all three $Pt_3Ni(hkl)$ crystals is pure Pt (Fig. 1B) [i.e., all form the so-called Pt-skin structures (*17*, *20*)]. Previous studies of PtNi single-crystal surfaces in UHV had indicated that this surface enrichment of Pt in the first layer is counterbalanced by its depletion in the next two to three atomic layers, so that the concentration profile oscillates around the bulk value (*24*, *25*). We demonstrated that segregation-driven near-surface compositional changes result in distinctive electronic properties of the PtNi(*hkl*) alloys.

The surface electronic structures were obtained from the background-corrected UPS spectra (*26*). As summarized in Fig. 1C, the *d*-band density of states (DOS) is structure-sensitive, and the position of the *d*-band center shifts from –2.70 eV on $Pt_3Ni(110)$ to –3.10 eV on $Pt_3Ni(111)$ to –3.14 eV on $Pt_3Ni(100)$. Furthermore, the DOS of the alloy surfaces is quite different from that of corresponding pure Pt single crystals; that is, on the (110), (100), and (111) alloy surfaces, the *d*-band center is downshifted by about 0.16, 0.24, and 0.34 eV, respectively. An important yet largely unexplored issue in surface electrochemistry on alloys is understanding how chemisorption energies correlate with the average energy of the *d*-state on the surface atoms to which the adsorbate binds (i.e., the ligand effect). To do this, we compared the results on the (111) surfaces with the same composition and arrangement of surface atoms but with a different *d*-band center position. Although we are highlighting how the difference between the electronic surface structures of Pt(111) and $Pt_3Ni(111)$ can affect the adsorption of spectator species and the kinetics of the ORR, the findings are generally applicable to other single-crystal alloy surfaces.

We next determined the stability of a surface after transfer from UHV into the electrochemical environment. Surface x-ray scattering (SXS) was used to characterize both the potential range of stability as well as the near-surface composition of the alloy in situ. Only results for $Pt_3Ni(111)$ are presented because they provide the most useful information about the potential-induced changes in the surface structure and segregation profile; a brief description of results for (110) and (100) can be found in (*27*). The termination of the $Pt_3Ni(111)$ lattice at the surface in terms of elemental composition and surface relaxation was determined by measurement and analysis of the crystal truncation rods (CTRs) (*28*). $Pt_3Ni(111)$ has the face-centered cubic (fcc) lattice with random occupation of sites by Pt and Ni, and this lattice gives rise to SXS similar to that obtained from a monocrystalline fcc lattice. Sensitivity to atomic layer composition is enhanced by the use of anomalous x-ray scattering techniques in which the incident x-ray energy is tuned to an atomic adsorption edge of the material (*29*). Thus, from SXS, we obtained information about the positions and compositions, both in the surface and subsurface layers. The CTR analysis shows that, at 0.05 V, the first layer is composed entirely of Pt and, whereas the second atomic layer is Ni-rich (52% of Ni as com-

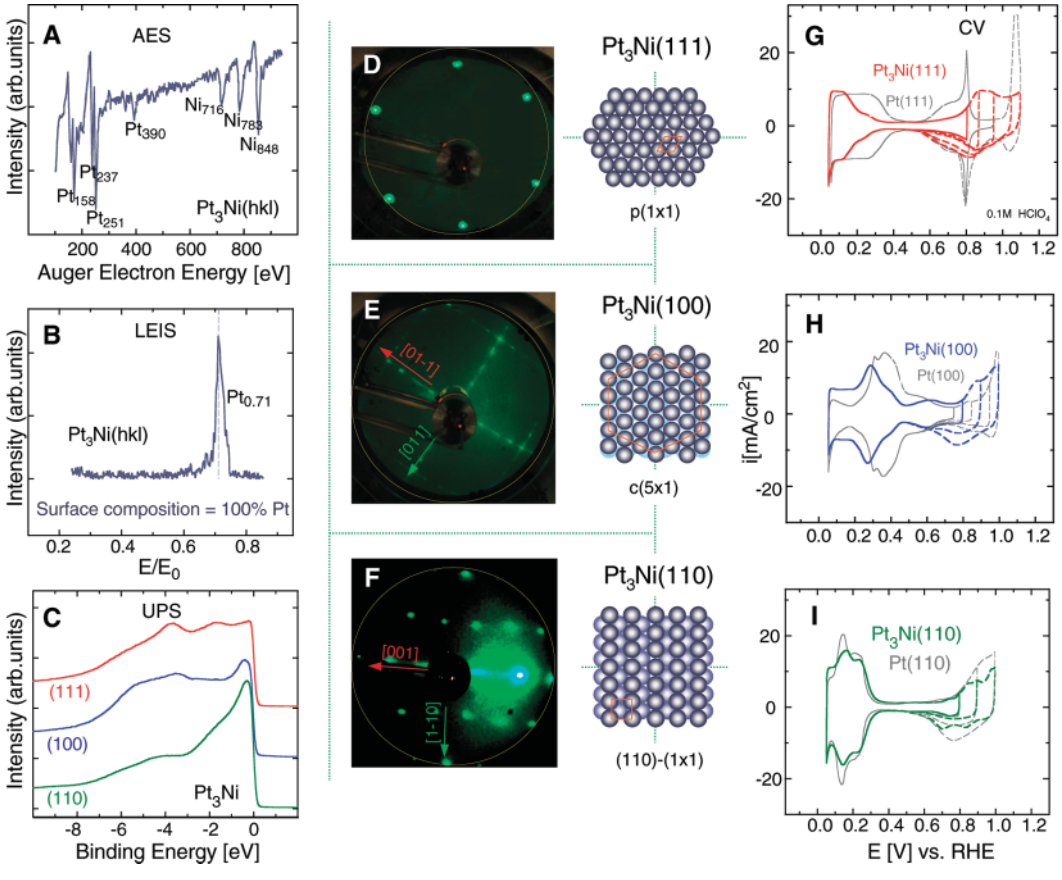

Fig. 1. Surface characterization of the Pt_3Ni single crystals in UHV and electrochemical environments. (**A**) AES spectra. (**B**) LEIS spectra. E/E_0, where E is energy of scattered electrons, and E_0 is the energy of the incident ion beam. (**C**) UPS spectra. (**D** to **F**) LEED patterns with corresponding ball models. (**G** to **I**) Cyclic voltammetry (CV) in $HClO_4$ (0.1 M) as compared to the voltammetry of the corresponding Pt single crystal (gray curves). RHE, reversible hydrogen electrode.

pared to 25% of Ni in the bulk), the third layer is again Pt-enriched (87%) (Fig. 2A). Having determined the near-surface structure at 0.05 V, the potential was cycled while the scattered x-ray intensity was measured at a CTR position that is sensitive to surface relaxation and surface roughness (Fig. 2A). We find that both the $Pt_3Ni(111)$ surface structure as well as the segregation profile are completely stable over this potential range because the changes in the x-ray scattering signal are fully reversible, and we find that the decrease in intensity at positive potential is consistent with an inward relaxation (contraction) of the surface atomic layer (this result is confirmed by similar measurements at other reciprocal lattice positions). The contraction of Pt surface atoms is induced by the adsorption of oxygenated species, which is determined by the Ni-induced modification of the Pt-skin electronic structure. A direct consequence of contraction of the topmost layer of Pt-skin at the potentials higher than 0.8 V is the increased stability of this surface over corresponding pure Pt(111), which was additionally confirmed by prolonged cycling in the designated potential range.

The relations between the surface electronic properties and the potential-dependent surface coverage by adsorbing species (the adsorption isotherms in Fig. 2C) were established by comparing the experimentally determined position of the *d*-band centers to the fractional coverages of adsorbed hydrogen ($H^+ + e^- = H_{upd}$, where H_{upd} refers to the underpotentially deposited hydrogen) between $0.05 < E < 0.4$ V, where E is the applied potential, and hydroxyl species ($2H_2O = OH_{ad} + H_3O^+ + e^-$, where OH_{ad} is the adsorbed hydroxyl layer) above 0.6 V (Fig. 2C). Careful inspection of the voltammograms in Fig. 2B revealed that on Pt(111)-skin, which consists of the same surface density of Pt atoms as Pt(111), a dramatic negative shift (≈0.15 V) in H_{upd} formation and positive shift (≈0.1 V) in OH_{ad} formation occurred relative to Pt(111). In agreement with the onset of adsorption, on $Pt_3Ni(111)$, the fractional coverages by H_{upd} and OH_{ad} (Θ_{Hupd} and Θ_{OHad}) were dramatically reduced by 50% relative to Pt(111), which is in agreement with the large downshift (0.34 eV) of the *d*-band center position on the Pt-skin structure. As shown in Fig. 1, H and I, similar changes occurred for the other two single-crystal surfaces. On the Pt(100)-skin, Θ_{Hupd} was reduced by ≈15% relative to Pt(100), and Θ_{OHad} was reduced by ≈25%. On $Pt_3Ni(110)$, small but clearly discernable decreases in Θ_{Hupd} (≈10%) and the fractional coverage by OH_{ad} (Θ_{OH}) (≈20%) were observed relative to Pt(110).

To describe these effects quantitatively, we performed DFT calculations, using pseudopotentials and a plane-wave basis set, on the adsorption of OH and H_2O at 0.25 monolayer coverage on modeled Pt(111) surfaces, with second atomic layers containing 0 or 50% Ni atoms. In acid solutions, OH_{ad} would react with H^+ and form H_2O on the catalyst surface. The change in the reversible potential ΔU° of the above reaction on Pt(111) resulting from sublayer Ni atoms is

$$\Delta U^\circ = [E_{ads}(OH)_{Pt} - E_{ads}(OH)_{PtNi} - E_{ads}(H_2O)_{Pt} + E_{ads}(H_2O)_{PtNi}]/F \quad (1)$$

Here, $E_{ads}(OH)_{Pt}$, $E_{ads}(H_2O)_{Pt}$, $E_{ads}(OH)_{PtNi}$, and $E_{ads}(H_2O)_{PtNi}$ are the adsorption energies of OH and H_2O on Pt(111) with or without sublayer Ni atoms, respectively, and F is the Faraday constant. The DFT calculations show a positive shift of $\Delta U^\circ = 0.10$ V when the sublayer has 50% Ni atoms. The experiment and theory thus reach an excellent and quantitative agreement in this case and clearly establish an electronic effect of subsurface Ni on the Pt-OH chemical bonding.

The ORR is a multielectron reaction ($^1/_2O_2 + 2H^+ + 2e^- = H_2O$) that may include a number of elementary steps involving different reaction intermediates (*7*, *30*). We proposed that the rate of the ORR can be expressed as

$$i = nFKc_{O_2}(1 - \Theta_{ad})^x \exp(-\beta FE/RT) \exp(-g\Delta G_{ad}/RT) \quad (2)$$

where i is the measured current; n, F, K, E, x, β, γ, and R are constants [(*3*); for definitions, see (*31*)] ; c_{O_2} is the concentration of O_2 in the solution, Θ_{ad} is the total surface coverage by adsorbed spectator species [hydroxyl and anions; for example, OH_{ad} (Θ_{OH}) and specifically adsorbed anions (Θ_{Aad})]; ΔG_{ad} is the Gibbs energy of adsorption of reactive intermediates, and T is temperature. In the derivation of Eq. 2, it is assumed that (i) the ORR takes place on electrodes that are modified by OH_{ad}, anions, etc., and (ii) the reactive intermediates (O_2^- and H_2O_2) are adsorbed to low coverage (i.e., they are not a substantial part of Θ_{ad}).

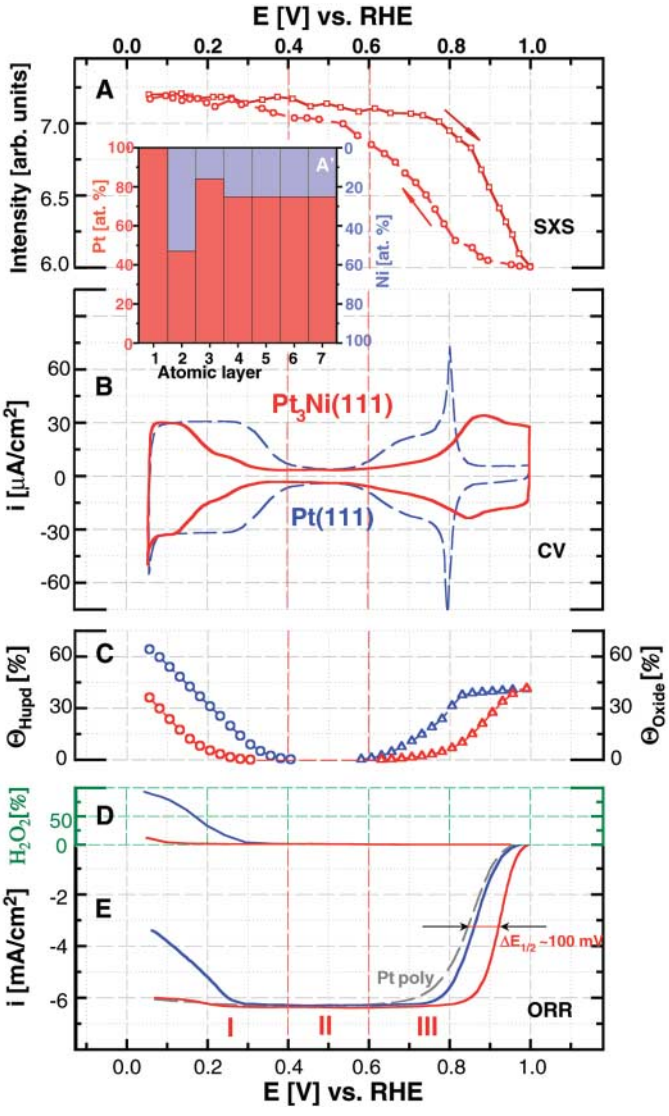

Fig. 2. In situ characterization of the $Pt_3Ni(111)$ surface in $HClO_4$ (0.1 M) at 333 K. (**A**) SXS data and (**A′**) concentration profile revealed from SXS measurements. at. %, atomic %. (**B**) Cyclic voltammetry in designated potential region (red curve) as compared to the voltammetry obtained from Pt(111) surface (blue curve). (**C**) Surface coverage calculated from cyclic voltammograms of $Pt_3Ni(111)$ (red curve) and Pt(111) (blue curve); polarization curves obtained from rotating ring disk electrode (RRDE) measurements. Θ_{Oxide}, surface coverage by adsorbed spectator oxygenated species. (**D**) Green scale refers to hydrogen peroxide production in designated potential region and (**E**) ORR currents measured on $Pt_3Ni(111)$ (red curve), Pt(111) (blue curve), and polycrystalline Pt (gray curve) surfaces. The arrows are showing the positive potential shift of 100 mV in electrode half-potential ($\Delta E_{1/2}$) between ORR polarization curves measured on Pt-poly and $Pt_3Ni(111)$ surfaces. I, II, and III represent potential region of H_{apd} adsorption/desorption processes, double-layer region, and region of OH_{ad} layer formation, respectively.

Based on these assumptions, the kinetics of O_2 reduction are determined by the number of free Pt sites available for the adsorption of O_2 (the $1 - \Theta_{ad}$ term in Eq. 2) and by the ΔG_{ad} of O_2 and reaction intermediates (the ΔG_{ad} term in Eq. 2) on metal surfaces precovered by OH_{ad}. We used this reaction pathway and rate expression first to analyze the effects of electronic properties on the kinetics of the ORR on $Pt_3Ni(111)$ and Pt(111) and then, by comparing activities on different $Pt_3Ni(hkl)$ surfaces, to establish structure sensitivity.

A characteristic set of polarization curves (the relation of i versus E) for the ORR on Pt-poly, Pt(111), and $Pt_3Ni(111)$ surfaces in $HClO_4$ (0.1 M) at 333 K is summarized in Fig. 2D. For all three surfaces, the polarization curves exhibit two distinguishable potential regions. By starting at 0.05 V and scanning the electrode potential positively, well-defined diffusion-limiting currents from 0.2 to 0.7 V are followed by a mixed kinetic-diffusion control region between $0.8 < E < 1.0$ V. Further inspection of Fig. 2D reveals that the ORR kinetic is accelerated on the Pt(111)-skin relative to Pt(111), causing the positive shift of 100 mV in the half-wave potential. Given that Θ_{OHad} is attenuated on the Pt-skin structure, the key parameter that determines the unusually catalytic activity of $Pt_3Ni(111)$ is the low coverage by OH_{ad} [i.e., the $(1 - \Theta_{OHad})$ term in the kinetic equation for the ORR]. Additional confirmation that the fractional coverages by spectator species are indeed controlling the kinetics of the ORR was found by analyzing the results in the potential region where the adsorption of hydrogen is taking place ($E < 0.2$ V). Because of the lower coverage by H_{upd}, the production of peroxide is substantially attenuated on the Pt-skin surface. At the fuel cell relevant potentials ($E > 0.8$ V), the observed catalytic activity for the ORR on $Pt_3Ni(111)$ is the highest that has ever been observed on cathode catalysts, including the $Pt_3Ni(100)$ and $Pt_3Ni(110)$ surfaces.

Synergy between surface geometry and surface electronic structure for the ORR is illustrated in Fig. 3. As summarized, the different low-index surfaces have markedly different activity for this reaction [that is, $Pt_3Ni(100)$-skin < $Pt_3Ni(110)$-skin <<< $Pt_3Ni(111)$-skin, with the change in activity between the least active (100) and the most active (111) surfaces being greater than an order of magnitude]. Structure sensitivity of the ORR on the Pt low-index single-crystal surfaces in perchloric acid has been well established (*3*), with activities increasing in the order Pt(100) << Pt(111) < Pt(110) (Fig. 3). These differences have been attributed to the structure-sensitive adsorption of OH_{ad} on $Pt(hkl)$ and its inhibiting (site blocking) effect on O_2 adsorption. In the potential region of OH adsorption, the structure sensitivity of the $Pt_3Ni(hkl)$-skin surfaces has the same origin.

In order to reveal the role of the electronic structure onto ORR kinetic, we compared electrodes with the same surface morphology. The most pronounced effect was observed on the (111) surfaces. For the same $p(1 \times 1)$ arrangement of the topmost layer, the same surface atomic density, and the same surface composition (100% Pt) but for a different electronic structure ($|\Delta d_{[111]}| = 0.34$ eV, where $|\Delta d_{[hkl]}|$ is the *d*-band center shift), the ORR is being enhanced by factor of 10 on Pt(111)-skin relative to that on Pt(111). Given that extended Pt surfaces have 5 to 10 times the activity per surface Pt atoms than the state-of-the-art Pt/C catalysts that are currently used in the PEMFC (~0.2 mA/cm^2 at 0.9 V) (*10*, *14*), a total 90-fold enhancement of Pt(111)-skin versus that of Pt/C has been achieved.

Considering that the $Pt_3Ni(111)$-skin surface exhibits the highest catalytic activity that has ever been detected, the challenge would be to create a nanocatalyst with electronic and morphological properties that mimic the $Pt_3Ni(111)$ surface. Therefore in the future, a way to reduce the current value (~1.0g of Pt per kW) of Pt-specific power density in a PEMFC without a loss in cell voltage, while also maintaining the maximum power density (W/cm^2), would be the engineering of $Pt_3Ni(111)$-skin–like nanocatalysts.

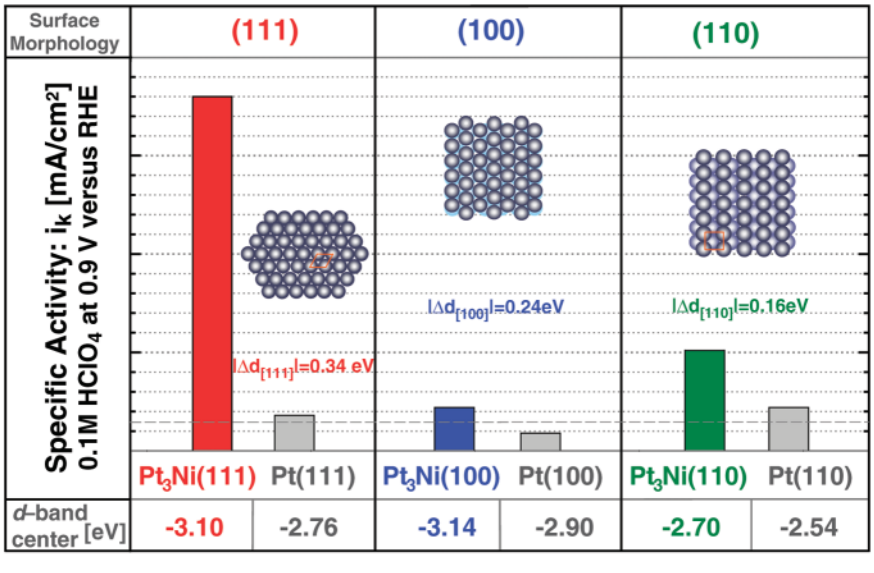

Fig. 3. Influence of the surface morphology and electronic surface properties on the kinetics of ORR. RRDE measurements for ORR in $HClO_4$ (0.1 M) at 333 K with 1600 revolutions per minute on $Pt_3Ni(hkl)$ surfaces as compared to the corresponding $Pt(hkl)$ surfaces (a horizontal dashed gray line marks specific activity of polycrystalline Pt) are shown. Specific activity is given as a kinetic current density i_k, measured at 0.9 V versus RHE. Values of *d*-band center position obtained from UPS spectra are listed for each surface morphology and compared between corresponding $Pt_3Ni(hkl)$ and $Pt(hkl)$ surfaces.

References and Notes

1. S. Gottesfeld, T. A. Zawodzinski, in *Advances in Electrochemical Science and Engineering*, R. C. Alkire, H. Gerischer, D. M. Kolb, C. W. Tobias, Eds. (Wiley-VCH, Weinheim, Germany, 1997), vol. 5.
2. F. Besenbacher *et al.*, *Science* **279**, 1913 (1998).
3. N. M. Markovic, P. N. Ross, *Surf. Sci. Rep.* **45**, 117 (2002).
4. W. Vielstich, A. Lamm, H. A. Gasteiger, *Handbook of Fuel Cells: Fundamentals, Technology, and Applications* (Wiley, West Sussex, UK, ed. 1, 2003).
5. J. K. Norskov, C. H. Christensen, *Science* **312**, 1322 (2006).
6. A. J. Appleby, *Catal. Rev.* **4**, 221 (1970).
7. M. R. Tarasevich, A. Sadkowski, E. Yeager, in *Comprehensive Treatise in Electrochemistry*, J. O. M. Bockris, B. E. Conway, E. Yeager, S. U. M. Khan, R. E. White, Eds. (Plenum, New York, 1983), chap. 6.
8. K. Kinoshita, *Electrochemical Oxygen Technology* (Wiley, New York, 1992).
9. R. R. Adzic, in *Electrocatalysis*, J. Lipkowski, P. N. Ross, Eds. (Wiley-VCH, New York, 1998).
10. H. A. Gasteiger, S. Kocha, B. Sompalli, F. T. Wagner, *Appl. Catal. B* **56**, 9 (2005).
11. F. J. Luczak, D. A. Landsman, U.S. Patent, 4,711,829 (1987).
12. S. Mukerjee, S. Srinivasan, *J. Electroanal. Chem.* **357**, 201 (1993).
13. T. Toda, H. Igarashi, H. Uchida, M. Watanabe, *J. Electrochem. Soc.* **146**, 3750 (1999).
14. U. A. Paulus *et al.*, *J. Phys. Chem. B* **106**, 4181 (2002).
15. V. Stamenkovic, T. J. Schmidt, N. M. Markovic, P. N. Ross Jr., *J. Phys. Chem. B* **106**, 11970 (2002).
16. J. Zhang, M. B. Vukmirovic, Y. Xu, M. Mavrikakis, R. R. Adzic, *Angew. Chem.* **117**, 2170 (2005).
17. V. R. Stamenkovic, B. S. Moon, K. J. J. Mayrhofer, P. N. Ross, N. M. Markovic, *J. Am. Chem. Soc.* **128**, 8813 (2006).
18. B. Hammer, J. K. Norskov, in *Advances in Catalysis* (Elsevier, Amsterdam, 2000), vol. 45, pp. 71–129.
19. J. Greeley, J. K. Norskov, M. Mavrikakis, *Annu. Rev. Phys. Chem.* **53**, 319 (2002).
20. V. Stamenkovic *et al.*, *Angew. Chem.* **45**, 2897 (2006).
21. C. T. Campbell, *Annu. Rev. Phys. Chem.* **41**, 775 (1990).
22. P. A. Thiel, P. J. Estrup, in *The Handbook of Surface Imaging and Visualization*, A. T. Hubbard, Ed. (CRC Press, Boca Raton, FL, 1995).
23. V. Stamenkovic, T. J. Schmidt, P. N. Ross, N. M. Markovic, *J. Electroanal. Chem.* **554-555**, 191 (2003).
24. Y. Gauthier, R. Baudoing, J. Rundgren, *Phys. Rev. B* **31**, 6216 (1985).
25. Y. Gauthier, *Surf. Rev. Lett.* **3**, 1663 (1996).
26. B. S. Mun, C. Lee, V. Stamenkovic, N. M. Markovic, P. N. Ross, *Phys. Rev. B* **71**, 115420 (2005).
27. For the other two single-crystal surfaces, we have also found that the Pt-skin layer that formed in UHV is stable in an electrochemical cell. Unlike the $Pt_3Ni(100)$/vacuum interface, however, the electrolyte interface was found to be unreconstructed at all potentials because of anion-induced adsorption. The SXS results for the $Pt_3Ni(110)$

surface are ambiguous [i.e., it was not clear whether the (1 × 2) phase was indeed transferred from UHV into an electrochemical cell]. Nevertheless, the SXS results clearly show that the surface is relatively smooth and stable, and thus reliable electrochemical results can be obtained on both electrodes.
28. I. K. Robinson, E. Vlieg, K. Kern, *Phys. Rev. Lett.* **63**, 2578 (1989).
29. C. A. Lucas, N. M. Markovic, in *Advances in Electrochemical Science and Engineering*, R. C. Alkire, D. M. Kolb, J. Lipkowski, P. N. Ross, Eds. (Wiley-VCH, Weinheim, Germany, 2006), vol. 9.
30. N. M. Markovic, H. A. Gasteiger, P. N. Ross, *J. Phys. Chem.* **99**, 3411 (1995).
31. In Eq. 2, n is the number of electrons; K is the rate constant; x is the order of active Pt sites; β and γ are the symmetry factors (which are assumed to be ½); and R is the universal gas constant.
32. N.M.M. and V.R.S. acknowledge the support from the contract (DE-AC02-06CH11357) between the University of Chicago Argonne, LLC, and the U.S. Department of Energy. We acknowledge the support of General Motors and helpful discussions with H. A. Gasteiger and F. T. Wagner. C.A.L. and B.F. acknowledge the support of the UK Engineering and Physical Sciences Research Council. V.R.S. thanks M. West for support in experimental design.

Supporting Online Material
www.sciencemag.org/cgi/content/full/1135941/DC1
Materials and Methods

5 October 2006; accepted 7 December 2006
Published online 11 January 2007;
10.1126/science.1135941
Include this information when citing this paper.

Water Catalysis of a Radical-Molecule Gas-Phase Reaction

E. Vöhringer-Martinez,[1] B. Hansmann,[1] H. Hernandez,[2] J. S. Francisco,[2] J. Troe,[1] B. Abel[1]*

There has been considerable speculation about the role of water and water complexes in chemical gas-phase reactions, including the conjecture that water may act as a molecular catalyst through its ability to form hydrogen bonds. Here, we present kinetic studies in which the effect of water on the rate of the reaction between hydroxyl radicals and acetaldehyde has been measured directly in Laval nozzle expansions at low temperatures. An increasing enhancement of the reaction rate by added water was found with decreasing temperatures between 300 and 60 kelvin. Quantum chemical calculations and statistical rate theory support our conclusions that this observation is due to the reduction of an intrinsic reaction barrier caused by specific water aggregation. The results suggest that even single water molecules can act as catalysts in radical-molecule reactions.

Water introduces many unusual features into the kinetics and energetics of chemical and biological reaction systems, which are difficult to rationalize on a molecular level (*1*, *2*). Beyond the well-known properties of bulk water, there is evidence that even single confined water molecules in molecular aggregates may have a decisive influence on gas phase chemistry (*3*). An intriguing question is whether water molecules can even act as true catalysts in chemical reactions, for example, through their ability to form hydrogen bonds. A number of molecule-water complexes have evidenced photochemistry distinct from that of the isolated molecules (*4*). Complexes of water with ozone (*5*), sulfuric acid (*6*), nitric acid (*7*), nitrous oxide (*8*), and chlorine dioxide (*9*–*11*) are examples of water aggregates that may be important in atmospheric photochemistry.

Beyond its ability to influence photochemistry, water is known to form complexes with active species such as radicals and polar molecules in thermal reactions (*4*, *12*, *13*), and such complexation may alter intrinsic reaction barriers in bimolecular reactions. In addition, the radical-complex mechanism (*14*) is well known to have a characteristic impact on recombination processes, which could be enhanced by water molecules. Last, water may act as a particularly efficient collision partner to collisionally stabilize intermediates of such reactions. Unfortunately, all these effects (hereafter referred to as the catalysis, the radical-complex, and the energy-transfer mechanisms) may influence overall reaction yields and rates in bimolecular reactions (*14*) and are often difficult to distinguish.

For example, there is experimental (*15*) and theoretical (*4*) evidence that the hydroperoxy radical (HO_2) forms a hydrogen-bonded complex with a water molecule, which has the potential to affect the kinetics of HO_2 reactions. Along these lines, the rate constant for the self-reaction of HO_2 to yield H_2O_2 and O_2, which proceeds via a long-lived intermediate, is somewhat faster in the presence of water than in its absence (*4*, *16*, *17*). A similar effect has been observed for the reaction of hydroperoxy radicals with nitrogen dioxide in the presence of water (*18*). However, the origin of the documented impact of water on the kinetics in general remains unclear. Although "prereaction" complexes of water in chemical reactions have been suggested in the past (*16*), a conclusive mechanism and a detailed kinetic analysis of the systems were not given. The general problem for an understanding of such kinetic systems is that they depend upon temperature, pressure, and specific molecular parameters and so require a detailed kinetic analysis using reaction rate theory and high-level quantum chemistry (*14*).

Following up on a long-standing conjecture that even single or few water molecules may alter energetics in general and reaction barriers in particular or favor reaction sites, the goal of this study was to investigate the role of water as a real catalyst in chemical gas-phase reactions potentially relevant for atmospheric chemistry and, in particular, to provide a clear example for a water-catalyzed radical-molecule reaction. The fast H-atom abstraction reaction of OH with acetaldehyde proved to be a good system for studying the effect of water aggregation on the kinetics. The reaction does not involve long-lived, strongly bound intermediates such as those found in other complex-forming bimolecular reactions, for example, in the reaction of OH with CO proceeding via HOCO complexes (*14*).

Recent experimental and theoretical work has provided evidence for the assumption that the reaction proceeds predominantly through abstraction of the aldehydic hydrogen atom (*19*–*22*). The addition of the OH radical to the double bond does not take place because its activation energy is much larger than that for hydrogen abstraction (*23*, *24*). In addition, the aldehydic hydrogen atom has a relatively small binding energy compared with that of hydrogen atoms in the methyl group. A prereactive complex $CH_3CHO\cdots HO$ has been postulated by D'Anna *et al*. (*24*) and Alvarez-Idaboy *et al*. (*23*), and its binding energy was estimated to be ≈18 kJ mol^{-1}. Although transient prereactive complexes have not been directly characterized experimentally, their presence has been identified indirectly in several radical-molecule reactions and associated with a negative temperature dependence of the reaction rate (*25*, *26*). Nielsen and co-workers calculated barriers (relative to the reactant energy) to aldehydic H abstraction, methyl H abstraction, and OH addition to the carbonyl bond of –14.2 kJ mol^{-1}, 12.1 kJ mol^{-1}, and 30.9 kJ mol^{-1}, respectively (*24*). A negative temperature dependence of the reaction rate at higher temperatures has also been reported (*22*) without a theoretical analysis of the effect.

We measured rates and rate constants for the OH + CH_3CHO reaction in the presence and absence of water vapor by using a pulsed Laval nozzle expansion (*25*, *27*) (Fig. 1A). The reaction was followed by laser-induced fluorescence (LIF) to monitor the decay of OH radical concentration. The rate constants were determined over a temperature range of 58 to 300 K. The decay profiles can be fitted well by an exponential time law (Fig. 1B). Plots of pseudo-first-order

[1]Institut für Physikalische Chemie der Universität Göttingen, Tammannstrasse 6, 37077 Göttingen, Germany. [2]Department of Chemistry and Department of Earth and Atmospheric Sciences, Purdue University, West Lafayette, IN 47907–2084, USA.

*To whom correspondence should be addressed. E-mail: babel@gwdg.de